

Charged Lepton EDM with Extra Yukawa Couplings

Wei-Shu Hou, Girish Kumar and Sven Teunissen

Department of Physics, National Taiwan University, Taipei 10617, Taiwan

In a two Higgs doublet model with extra Yukawa couplings, we assess the new physics contributions to charged lepton electric dipole moment. We focus especially on muon (and tau) EDM where in the coming decade several experiments — Muon $g-2$, J-PARC and PSI (and Belle II) — will push sensitivities down by several orders of magnitude. With the working assumption that extra Yukawa couplings are analogous to SM ones in strength and taking exotic scalar masses in sub-TeV range, we find that μ and τ EDM can be enhanced to values larger than new physics scenarios that scale with lepton mass. The main effect comes from the flavor-conserving extra top coupling ρ_{tt} via well-known two-loop diagrams. Deviating from our working assumption, if the muon $g-2$ anomaly arises from the one-loop diagram, driven by singly enhanced lepton flavor violating $\rho_{\tau\mu}$ coupling, it can also induce rather large muon EDM, accessible at upcoming experiments.

I. INTRODUCTION

All charged-parity violation (CPV) observed in the laboratories so far are in the quark sector. The Cabibbo-Kobayashi-Maskawa (CKM) matrix [1, 2] that govern the weak interactions of the Standard Model (SM) has been impressively successful in accounting for all such effects. But, as is known, the KM phase does not provide enough CPV to satisfy the Sakharov condition [3] for the disappearance of antimatter in the Universe. Various new physics (NP) models attempt to make up for this by supplying new complex phases to hopefully explain the baryon asymmetry of the Universe (BAU).

The general two Higgs doublet model (g2HDM) [4, 5], also known as 2HDM Type-III [6], is attractive in this context. In g2HDM, one does not introduce a Z_2 symmetry to enforce Natural Flavor Conservation [7]. Thus, the second Higgs doublet brings in extra Yukawa coupling matrices, which are in general *complex*. The new phases, especially those associated with extra top quark couplings, ρ_{tt} and ρ_{tc} , which are likely the stronger in strength, can drive electroweak baryogenesis (EWBG) and explain BAU [8, 9]. Complex extra Yukawa couplings can also contribute to CPV observables accessible in the laboratory, such as charged lepton electric dipole moment (ℓ EDM), which we denote as d_ℓ .

Lepton EDMs are powerful probes of NP CPV. The SM predictions for ℓ EDM are extremely tiny (e.g. $|d_e| \sim 10^{-38}$ e cm [10–12]) because the sole complex phase, the KM phase, survives only at the four-loop level. With essentially no SM background, detection of ℓ EDM will establish the presence of NP of CPV nature.

Recently, there has been very good progress in the search for e EDM. The ACME experiment exploits the large internal electric field of ThO molecules to measure e EDM. Already in 2013, ACME provided the best upper limit on e EDM, $|d_e| < 8.7 \times 10^{-28}$ e cm [13]. Impressively, the bound was further improved to [14]

$$|d_e| < 1.1 \times 10^{-29} \text{ e cm, (ACME 2018)} \quad (1)$$

which is the best upper limit on any EDM. The bound of Eq. (1) puts stringent constraint on any BSM model

that seek to address the BAU problem.

For g2HDM, consistency with Eq. (1) has helped shed light on the structure of extra Yukawa couplings. As noted in Ref. [9], one can accommodate EWBG in g2HDM with flavor conserving coupling $|\rho_{tt}| \gtrsim 0.1$ (see Ref. [8] for flavor violating coupling ρ_{tc} which is immune to e EDM constraint), but parameter space with single coupling scenario runs into trouble with the ACME 2018 bound. This can be avoided by introducing extra electron Yukawa coupling ρ_{ee} , which helps salvage parameter space favorable for EWBG. Interestingly, the organization of these couplings follow the pattern [9],

$$|\rho_{ee}/\rho_{tt}| \propto \lambda_e/\lambda_t, \quad (2)$$

suggesting that the extra ρ couplings of g2HDM have similar hierarchical structure as Yukawa couplings in SM. Eq. (2) provides not only an elegant way of complying with the ACME 2018 bound, it connects EWBG with tiny CPV effects in the laboratories, such as e EDM.

Seeing that e EDM is highly sensitive to extra Yukawa couplings, in this paper we wish to explore the detailed contributions of extra Yukawa couplings to μ and τ EDM. Such an investigation is well-timed for the muon, where the Fermilab Muon $g-2$ experiment [15] has affirmed recently the significant deviation from SM expectation in a related observable — the anomalous magnetic moment of the muon. Any NP in muon $g-2$ certainly can have important implications for μ EDM, as we will show later.

The current bound on μ EDM is by the Muon $g-2$ experiment at Brookhaven National Laboratory (BNL) [16],

$$|d_\mu| < 1.8 \times 10^{-19} \text{ e cm, (BNL 2008)} \quad (3)$$

while an indirect limit, extracted from e EDM bound of ACME 2018, is claimed [17] at $\sim 2 \times 10^{-20}$ e cm. In the coming years, several experiments will search for μ EDM and improve Eq. (3). The Fermilab Muon $g-2$ [18] and the J-PARC muon $g-2$ /EDM [19] experiments project sensitivities at $\sim 10^{-21}$ e cm. Another experiment being planned at PSI [20] aims at improving by at least another order of magnitude, eventually reaching a sensitivity of 6×10^{-23} e cm. Thus, prospects for μ EDM in the coming decade appears promising.

lepton (ℓ)	Current bound ($e\text{cm}$)	Future sensitivity ($e\text{cm}$)
electron	1.1×10^{-29} (ACME [14])	-volatile-
muon	1.8×10^{-19} (BNL [16]) $\sim 2 \times 10^{-20}$ (Pospelov [17])	$\sim 10^{-21}$ (FNAL [18], J-PARC [19]) $\sim 6 \times 10^{-23}$ (PSI [20])
tau	$\text{Re } d_\tau = (-0.62 \pm 0.63) \times 10^{-17}$ (Belle [22]) $\text{Im } d_\tau = (-0.40 \pm 0.32) \times 10^{-17}$ (Belle [22])	$\sim 10^{-18}$ – 10^{-19} (Belle II [23]) $\sim 0.7 \times 10^{-19}$ (Bernreuther [24]) $\sim 10^{-18}$ – 10^{-19} (Belle II [23]) $\sim 0.4 \times 10^{-19}$ (Bernreuther [24])

TABLE I. Present bounds and future sensitivities for EDM of charged leptons, $|d_\ell|$.

Compared to e EDM and μ EDM, τ EDM measurement is hampered by the short τ lifetime. The present limits are derived from spin-momentum correlations of final state decay products in $e^+e^- \rightarrow \gamma^* \rightarrow \tau^+\tau^-$, where τ EDM enters the matrix element of the $\gamma\tau\tau$ vertex. An old limit of the Belle experiment [21] with 29.5 fb^{-1} was very recently updated [22] to full dataset of 833 fb^{-1} . These limits on the real and imaginary parts of d_τ , at $\sim 10^{-17} e\text{cm}$, can be read off Table I. An indirect bound extracted from e EDM [17] seems much better, but real and imaginary parts were not separately given. Belle II [23] should improve the bound by more than an order of magnitude. Furthermore, some improvement is possible by studying ‘‘optimal’’ observables [24].

If one assumes that the NP contribution scales as m_ℓ , such as models with [25] minimal flavor violation (MFV), one expects $|d_\mu/d_e| \simeq m_\mu/m_e$. Taking the current limit on e EDM of Eq. (1), d_μ is expected at only $\sim 2 \times 10^{-27} e\text{cm}$. A glance at Table I shows that future sensitivities fall short by more than four orders of magnitude, and it is even farther away for d_τ . But this m_ℓ scaling may not hold in NP models where the underlying flavor dynamics is quite different [26, 27], and the situation need not be as *pessimistic*. The g2HDM provides a simple example where extra Yukawa couplings can give much larger d_μ and d_τ . We will show that, in a scenario favored by the muon $g-2$ anomaly, very large d_μ that can be probed in the coming years is possible.

This paper is organized as follows. In the next section, we give the extra Yukawa interactions in g2HDM and our working assumptions for their strength. We then discuss μ EDM in Sec. III and present results for the one- and two-loop contributions, while in Sec. IV we analyze τ EDM in a similar fashion. In Sec. V, we discuss extra Yukawa couplings that violate our working assumptions, as possibly hinted by muon $g-2$, and discuss implications for EDM of all three charged leptons. Finally, we offer our conclusion in Sec. VI.

II. PRELIMINARIES

Before we proceed to the specifics, let us lay out the framework of the model. The Yukawa interactions in

g2HDM are given by [5, 28],

$$\begin{aligned}
\mathcal{L} = & -\frac{1}{\sqrt{2}} \sum_{f=u,d,\ell} \bar{f}_i \left[(\lambda_i^f \delta_{ij} s_\gamma + \rho_{ij}^f c_\gamma) h \right. \\
& + (\lambda_i^f \delta_{ij} c_\gamma - \rho_{ij}^f s_\gamma) H - i \text{sgn}(Q_f) \rho_{ij}^f A \left. \right] R f_j \\
& - \bar{u}_i [(V \rho^d)_{ij} R - (\rho^{u\dagger} V)_{ij} L] d_j H^+ \\
& - \bar{\nu}_i \rho_{ij}^\ell R \ell_j H^+ + h.c., \tag{4}
\end{aligned}$$

where $L(R) = (1 \mp \gamma_5)/2$ are projection operators, Q_f is the charge of fermion f in units of e , and V is the CKM matrix. The shorthand $c_\gamma \equiv \cos \gamma$ and $s_\gamma \equiv \sin \gamma$ represent mixing between two CP even scalars, h and H , which is known to be very small.

Although ρ_{ij} couplings are generic and do not possess information about SM Yukawa couplings λ_i , it is intriguing that data suggest the ρ matrices imitate closely the hierarchical structure of SM Yukawa matrices (see Eq. (2)), as already mentioned in the Introduction. The $\Delta F = 2$ processes such as $B_{s(d)} - \bar{B}_{s(d)}$ and $K^0 - \bar{K}^0$ mixing constrain off-diagonal entries of down-type ρ^d to very small values [29], which indicates that ρ^d is nearly diagonal. On the other hand, the extra top Yukawa coupling ρ_{tt} , important for our study, is allowed to be significant in strength [30]. For the lepton sector, the $\rho_{\ell\ell'}$ coupling related to third and second generation are tightly constrained from LFV decays $h \rightarrow \tau\mu$ and $\tau \rightarrow \mu\gamma$, but with $\rho_{tt} \sim 1$, values of $\rho_{\tau\mu} = \rho_{\mu\tau} \lesssim \mathcal{O}(\lambda_\tau)$ are easily allowed even for $c_\gamma \sim 0.1$ [31].

With these arguments in mind, we assume the following strengths for ρ_{ij} related to u - and ℓ -type matrices [32],

$$\rho_{ii} \lesssim \mathcal{O}(\lambda_i); \quad \rho_{1i} \lesssim \mathcal{O}(\lambda_1); \quad \rho_{3j} \lesssim \mathcal{O}(\lambda_3) \quad (j \neq 1), \tag{5}$$

where the first two conditions can also be applied to elements of the ρ^d matrix. Down-type couplings, however, do not play much role in our discussion, so Eq. (5) will be our working assumption while estimating the typical size of ℓ EDM in g2HDM. But we note that deviation from Eq. (5) is possible. For example, NP in muon $g-2$ may call for large deviation from the last condition in Eq. (5) for interpretation in 2HDM [38]. We will discuss in Sec. V the implications of such a scenario for ℓ EDM and assess the impact on our results.

It is worth pointing out that with $c_\gamma \lesssim 0.1$ our assumptions $\rho_{\mu\mu} \lesssim \mathcal{O}(\lambda_\mu)$ and $\rho_{\tau\tau} \lesssim \mathcal{O}(\lambda_\tau)$ are easily compatible with the latest data on di-muon and di-tau decays of the h boson, respectively. These processes provide access to the strength and phase of extra Yukawa couplings. Both ATLAS [33] and CMS [34] have reported the $h \rightarrow \mu\mu$ branching fraction relative to SM at 1.2 ± 0.6 and $1.19_{-0.39-0.14}^{+0.40+0.15}$, respectively. The $h\mu\mu$ coupling in Eq. (4) induces the following modification in g2HDM,

$$\frac{\mathcal{B}(h \rightarrow \mu\mu)}{\mathcal{B}(h \rightarrow \mu\mu)_{\text{SM}}} = \left| s_\gamma + c_\gamma \text{Re} \frac{\rho_{\mu\mu}}{\lambda_\mu} \right|^2 + \left| c_\gamma \text{Im} \frac{\rho_{\mu\mu}}{\lambda_\mu} \right|^2. \quad (6)$$

For $c_\gamma = 0.1$ and $\text{Re} \rho_{\mu\mu} = \text{Im} \rho_{\mu\mu} = \lambda_\mu/\sqrt{2}$, Eq. (6) gives $\simeq 1.14$, consistent with data.

The $h \rightarrow \tau\tau$ process provides an avenue for the study of CP properties of the h boson at the LHC (see e.g. Refs. [35, 36]). Very recently, CMS [37] has carried out a study of the CP structure of the $h\tau\tau$ coupling with 137 fb^{-1} data, reporting the phase of the τ Yukawa coupling, $\phi_{\tau\tau}$, at $4^\circ \pm 17^\circ (\pm 36^\circ)$ at the 68% (95%) C.L., with rather large errors. In the notation of Ref. [37], the $h\tau\tau$ coupling in Eq. (4) gives,

$$\tan \phi_{\tau\tau} = \frac{c_\gamma \text{Im} \rho_{\tau\tau}}{s_\gamma \lambda_\tau + c_\gamma \text{Re} \rho_{\tau\tau}}. \quad (7)$$

For $c_\gamma = 0.1$ with $\text{Re} \rho_{\tau\tau} = \text{Im} \rho_{\tau\tau} = \lambda_\tau/\sqrt{2}$, we find $\phi_{\tau\tau} \simeq 3.8^\circ$, which is compatible with data. A more precise measurement of $\phi_{\tau\tau}$ in the future could constrain this extra τ Yukawa coupling.

III. μ EDM

The EDM, d_ℓ , of lepton ℓ is defined through the effective Lagrangian,

$$\mathcal{L}_{\text{eff}}^{\text{EDM}} = -\frac{i}{2} d_\ell \bar{\ell} \sigma_{\alpha\beta} \gamma_5 \ell F^{\alpha\beta}, \quad (8)$$

where $\sigma_{\alpha\beta} = i[\gamma_\alpha, \gamma_\beta]/2$, and $F^{\alpha\beta}$ is the electromagnetic field strength tensor.

In g2HDM, the first finite contribution to ℓ EDM appears at one-loop. A sample one-loop diagram for μ EDM in g2HDM is given in Fig. 1. The dipole operator in Eq. (8) is chirality violating, so an additional mass insertion is required on the fermion line to obtain the correct chiral structure. This means that analogous diagrams

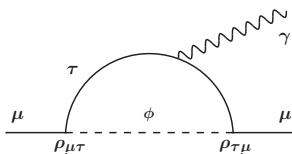


FIG. 1. One-loop diagram for μ EDM.

with lighter leptons in the loop are chirally suppressed, and we neglect them. Fig. 1 gives [39],

$$d_\mu|_{1\text{-loop}} \simeq -e \frac{m_\tau}{32\pi^2} \text{Im}(\rho_{\tau\mu}\rho_{\mu\tau}) \left[c_\gamma^2 \frac{\log x_{h\tau} - 3/2}{m_h^2} + s_\gamma^2 \frac{\log x_{H\tau} - 3/2}{m_H^2} - \frac{\log x_{A\tau} - 3/2}{m_A^2} \right], \quad (9)$$

where $x_{ij} = m_i^2/m_j^2$.

We note that the contribution of the h boson is negligible in Eq. (9) because $c_\gamma^2 \ll 1$, while the contributions of CP even and odd scalars have a relative sign between them, indicating that in the H - A degeneracy limit, one-loop contributions will be highly suppressed, which is indeed the case. For example, taking $c_\gamma = 0.1$ and $m_H = m_A = 300 \text{ GeV}$, we get $|d_\mu| \simeq 4 \times 10^{-22} |\text{Im}(\rho_{\tau\mu}\rho_{\mu\tau})| e \text{ cm}$. With $|\rho_{\tau\mu}| = |\rho_{\mu\tau}| \lesssim \lambda_\tau$, Eq. (5), we obtain $|d_\mu| \lesssim 4 \times 10^{-26} e \text{ cm}$ at one-loop, which is three orders of magnitude below PSI sensitivity. With m_A and m_H sufficiently apart, the one-loop contribution increases, but it remains outside of experimental reach. For example, with $m_H = 300 \text{ GeV}$ and $m_A = 500 \text{ GeV}$ and keeping other values as before, we obtain $|d_\mu| \lesssim 7 \times 10^{-25} e \text{ cm}$. Thus, we find that our working assumption of $\rho_{\ell\ell'}$ in Eq. (5) renders the one-loop contribution too small. Next, we consider two-loop diagrams — also known as Barr-Zee or Bjorken-Weinberg diagrams [40, 41].

It is well known that, despite having additional loop suppression, certain two-loop diagrams can dominate over one-loop diagrams. This can be understood qualitatively by noting that Fig 1 contains three chirality flips while only one flip in Fig. 2, which can let the latter compensate for the additional loop factor ($\sim \alpha/\pi$). Barr and Zee [40] calculated neutral scalar contributions with top quark and gauge bosons in the loop, which was later extended [42–46] to include other two-loop diagrams.

Following the convention used in Ref. [9], we categorize two-loop contributions to μ EDM into three parts,

$$d_\mu|_{2\text{-loop}} = d_\mu^{\phi\gamma} + d_\mu^{\phi Z} + d_\mu^{H^\pm W^+}, \quad (10)$$

related to effective $\phi\gamma\gamma$, $\phi\gamma Z$ and $H^\pm\gamma W^+$ vertices, respectively, as in Fig 2.

For $d_\mu^{\phi\gamma}$ with fermions in the loop, the dominant contribution comes from the top quark. For convenience, it

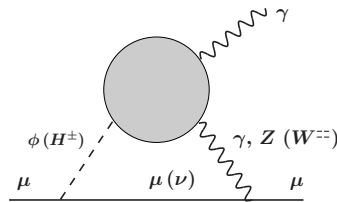


FIG. 2. Typical two-loop diagram for μ EDM, where ϕ (H^\pm) is a neutral (charged) scalar, and the gray blob stands for fermion, gauge, or scalar loop depending on the attached legs.

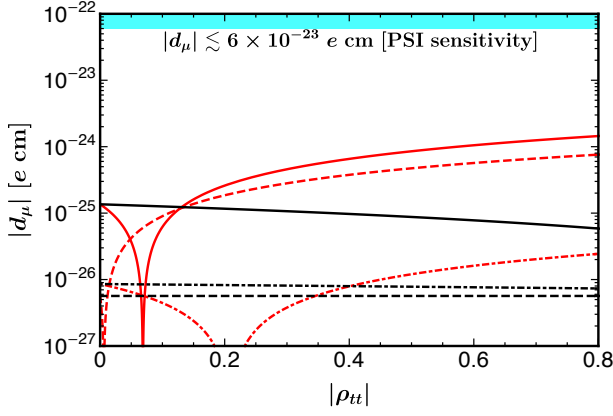


FIG. 3. Different two-loop contributions to $|d_\mu|$ as function of ρ_{tt} , with $c_\gamma = 0.1$, $m_H = m_A = m_{H^\pm} = 300$ GeV, and $\rho_{\mu\mu} = i\lambda_\mu$ for illustration. Red (black) curves correspond to $\phi_{tt} = 0$ ($\pi/2$). Solid, dashed, and dot-dashed curves represent contributions of $|d_\mu^{\phi\gamma}|$, $|d_\mu^{H^+W^+}|$, and $|d_\mu^{\phi Z}|$, respectively.

is written as the sum of two terms [9],

$$(d_\mu^{\phi\gamma})_t = (d_\mu^{\phi\gamma})_t^{\text{mix}} + (d_\mu^{\phi\gamma})_t^{\text{extra}} \quad (11)$$

where

$$\begin{aligned} (d_\mu^{\phi\gamma})_t^{\text{mix}} &= \frac{e\alpha s_\gamma c_\gamma}{6\sqrt{2}\pi^3 v} \left[\text{Im} \rho_{\mu\mu} \Delta f(x_{th}, x_{tH}) \right. \\ &\quad \left. + \frac{m_\mu}{m_t} \text{Im} \rho_{tt} \Delta g(x_{th}, x_{tH}) \right], \quad (12) \\ (d_\mu^{\phi\gamma})_t^{\text{extra}} &= \frac{e\alpha}{12\pi^3 m_t} \\ &\times \left\{ \text{Im} \rho_{\mu\mu} \text{Re} \rho_{tt} [c_\gamma^2 f(x_{th}) + s_\gamma^2 f(x_{tH}) + g(x_{tA})] \right. \\ &\quad \left. + \text{Re} \rho_{\mu\mu} \text{Im} \rho_{tt} [c_\gamma^2 g(x_{th}) + s_\gamma^2 g(x_{tH}) + f(x_{tA})] \right\}. \quad (13) \end{aligned}$$

where $\Delta f(a, b) = f(a) - f(b)$, $\Delta g(a, b) = g(a) - g(b)$, and loop functions $f(x)$ and $g(x)$ are given in Appendix A. Note that for $x \sim 1$, $f(x), g(x) \sim x$, and for small x , $f(x), g(x) \sim x(\log x)^2/2$, which further exemplifies why the top quark diagram is dominant.

Eq. (12) is due to mixing of SM Yukawa couplings with extra Yukawa couplings, and therefore has a linear dependence on $\text{Im} \rho_{ii}$ with no dependence on m_A . On the other hand, Eq. (13) contains contributions from extra Yukawa couplings only. For very small c_γ , the ‘‘mix’’ term becomes negligible, and the top loop contribution $(d_\mu^{\phi\gamma})_t \simeq (d_\mu^{\phi\gamma})_t^{\text{extra}}$ is governed by Eq. (13). One also notes that, for $\rho_{\mu\mu}$ and ρ_{tt} both purely real or purely imaginary, Eq. (13) does not contribute, which yields $(d_\mu^{\phi\gamma})_t \simeq (d_\mu^{\phi\gamma})_t^{\text{mix}}$.

The diagram with W^+ in the loop induces contribution to $d_\mu^{\phi\gamma}$ for finite c_γ . Defining the $\phi W^+ W^-$ coupling as $i g m_W C_{\phi WW}$ [47, 48], where $C_{hWW} = s_\gamma$, $C_{HW^+ W^-} = c_\gamma$, and $C_{AW^+ W^-} = 0$, the diagram gives,

$$(d_\mu^{\phi\gamma})_W = -\frac{e\alpha s_\gamma c_\gamma}{32\sqrt{2}\pi^3 v} \text{Im} \rho_{\mu\mu} [I_\gamma(m_h) - I_\gamma(m_H)], \quad (14)$$

with loop function $I_\gamma(a)$ given in Appendix A. This diagram has sign opposite the top-loop, hence large cancellation can occur in some parameter space for finite c_γ . The cancellation is, however, sensitive to complex phases of extra Yukawa couplings.

Adding Eqs. (11) and (14) and taking $c_\gamma = 0.1$, $m_H = m_A = 300$ GeV, we illustrate $d_\mu^{\phi\gamma}$ as solid lines in Fig. 3 vs ρ_{tt} coupling. We take $|\rho_{\mu\mu}| = \lambda_\mu$ in accordance of Eq. (5) and assume it to be purely imaginary. The red (black) lines correspond to purely real (imaginary) ρ_{tt} . For $\phi_{tt} = 0$, as ρ_{tt} increases, top-loop diagram starts to compete with W -loop, resulting in cancellation between the two, seen as the dip in the plot. For larger values of ρ_{tt} , the top-loop overwhelms the W -loop, thereby bringing $d_\mu^{\phi\gamma}$ to $\sim 10^{-24}$ e cm. For $\phi_{tt} = \pi/2$, $(d_\mu^{\phi\gamma})_t$ is given by Eq. (12) only, where the ρ_{tt} term is suppressed further by m_μ , hence $(d_\mu^{\phi\gamma})_t$ is feebly sensitive to ρ_{tt} and never overpowers W -loop even for large $|\rho_{tt}| \sim 1$.

For $d_\mu^{\phi Z}$, one simply replaces the inner photon propagator (one connecting loop with muon line) with the Z propagator. By parity, only the vector part of $Z\mu\mu$ coupling contributes. Its smallness, together with $1/m_Z^2$ from the Z propagator, the $d_\mu^{\phi Z}$ effect is typically suppressed with respect to $d_\mu^{\phi\gamma}$. The corresponding formulae are relegated to Appendix A. In Fig. 3, $d_\mu^{\phi Z}$ are given as dot-dashed lines, with color coding as before. For both red and black lines, $|d_\mu^{\phi Z}|$ always lie far lower than $|d_\mu^{\phi\gamma}|$, except near cancellation regions of $|d_\mu^{\phi\gamma}|$.

On the other hand, complex extra Yukawa couplings of charged Higgs boson in Eq. (4) contribute significantly to $d_\mu^{H^+W^+}$. The main effect comes from top-bottom in the loop, which gives [45],

$$\begin{aligned} (d_\mu^{H^+W^+})_{t/b} &= -\frac{3e\alpha |V_{tb}|^2 \text{Im}(\rho_{tt}\rho_{\mu\mu})}{128\pi^3 m_t \sin^2 \theta_W} \\ &\times \left[Q_t F_t(x_{\phi t}, x_{Wt}) + Q_b F_b(x_{\phi t}, x_{Wt}) \right], \quad (15) \end{aligned}$$

where ϕ stands for H^+ only, and functions $F_q(a, b)$ are given in Appendix A.

Diagrams with W^+ and scalars in the loop were calculated in Ref. [46]. Adapting to our case, we find,

$$\begin{aligned} (d_\mu^{H^+W^+})_W &= -\frac{e\alpha s_\gamma c_\gamma \text{Im} \rho_{\mu\mu}}{128\sqrt{2}\pi^3 v \sin^2 \theta_W} \\ &\times \left[\mathcal{I}_4(m_h, m_{H^+}) - \mathcal{I}_4(m_H, m_{H^+}) \right], \quad (16) \end{aligned}$$

where $\mathcal{I}_4(a, b)$ is given in Appendix A.

Combining Eqs. (15) and (16), we give $d_\mu^{H^+W^+}$ in Fig. 3 as dashed lines, taking the same values of scalar masses and c_γ as before. For $\phi_{tt} = 0$ (red), $d_\mu^{H^+W^+}$ is basically governed by Eq. (15) and slightly lower than $d_\mu^{\phi\gamma}$, but significantly larger than $d_\mu^{\phi W}$. At $\rho_{tt} = 0$, the origin, $d_\mu^{H^+W^+}$ is given by Eq. (16), which lies between 10^{-27} – 10^{-26} e cm. For extremely tiny ρ_{tt} , the effects from Eqs. (15) and (16) tend to cancel. This behavior

is similar to the case of $d_\mu^{\phi\gamma}$ discussed previously. For $\phi_{tt} = \pi/2$ (black), there is no dependence on ρ_{tt} and the total contribution is given by Eq. (16), which is represented as a horizontal black dashed line.

We see from Fig. 3 that, our working assumption of Eq. (5) suggests μ EDM in g2HDM can be enhanced to $\sim 10^{-24}$ e cm. This, however, lies out of reach of muon $g-2$ experiments at FNAL and J-PARC by three orders of magnitude. Even with improved sensitivity at PSI, shown as cyan band in Fig. 3, it cannot probe extra Yukawa couplings with strength as given in Eq. (5).

Some comments are in order. There are additional subdominant diagrams related to charged Higgs loops which depend on trilinear Higgs couplings. The expressions of these are given in Appendix A. We ignore them since our scope is to cover effects from Yukawa interactions of Eq. (4). These contribution can be important in models with CPV scalar potentials, or 2HDM models with softly broken Z_2 symmetry, where large contributions such as in Eq. (15) are negligible (see e.g. Refs. [46, 49–52]). For the former case, we should mention that there are additional so-called “kite diagrams”, calculated recently in Ref. [51], which are required to obtain a gauge-invariant result.

IV. τ EDM

The diagrams contributing to τ EDM is similar to μ EDM, except a more significant coupling $\rho_{\tau\tau} \sim \lambda_\tau$ is involved, hence one would expect further enhancement.

One obtains the one-loop effect for τ EDM by replacing “ μ ” \rightarrow “ τ ” in Fig. 1. Diagrams with internal μ and e are again neglected because of chiral suppression. Since the flavor conserving $\phi\tau\tau$ vertex is involved, the SM Yukawa λ_τ also contributes via interference with $\rho_{\tau\tau}$. Using the results of Ref. [29], the one-loop contribution is

$$d_\tau \simeq -\frac{e m_\tau}{32\pi^2} \times \left\{ [s_{2\gamma}\lambda_\tau \text{Im } \rho_{\tau\tau} + c_\gamma^2 \text{Im } \rho_{\tau\tau}^2] \frac{\log x_{h\tau} - 3/2}{m_h^2} + [-s_{2\gamma}\lambda_\tau \text{Im } \rho_{\tau\tau} + s_\gamma^2 \text{Im } \rho_{\tau\tau}^2] \frac{\log x_{H\tau} - 3/2}{m_H^2} - \text{Im } \rho_{\tau\tau}^2 \frac{\log x_{A\tau} - 3/2}{m_A^2} \right\}. \quad (17)$$

In the small c_γ limit, λ_τ effects decouple. Taking $c_\gamma = 0.1$, $m_H = m_A = 300$ GeV, and $\text{Re } \rho_{\tau\tau} = \text{Im } \rho_{\tau\tau} \leq \lambda_\tau/\sqrt{2}$ for τ coupling following Eq. (5), we find $|d_\tau| \lesssim 6 \times 10^{-25}$ e cm, which is about five orders below Belle II projections. For $m_H = 300$ GeV and $m_A = 500$ GeV, the one-loop contribution increases to $|d_\tau| \lesssim 1.3 \times 10^{-24}$ e cm, but remains out of Belle II reach.

The discussion of two-loop contribution to d_τ is analogous to d_μ in Sec. III. Therefore, similar to Eq. (10), we write for d_τ at two-loop,

$$d_\tau|_{2\text{-loop}} = d_\tau^{\phi\gamma} + d_\tau^{\phi Z} + d_\tau^{H^+W^+}, \quad (18)$$

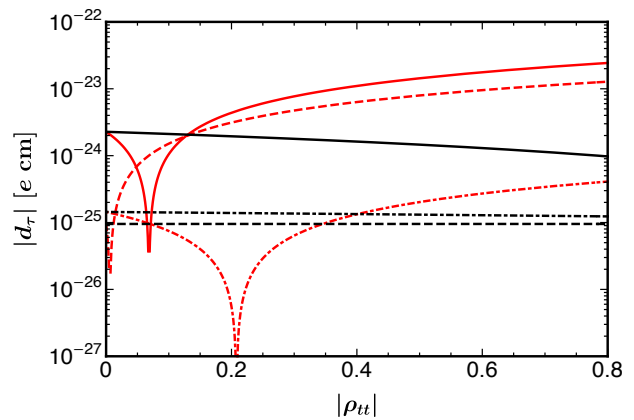


FIG. 4. Different two-loop contributions to $|d_\tau|$ as function of ρ_{tt} , taking $\rho_{\tau\tau} = i\lambda_\tau$. Color coding is the same as in Fig. 3.

where expressions for each term can be obtained from Eqs. (11) and (14)-(16) by change of label “ μ ” \rightarrow “ τ ”.

In Fig. 4 we give results for each term in Eq. (18) as functions of ρ_{tt} . The same benchmarks are used as in previous section: $m_H = m_A = m_{H^\pm} = 300$ GeV, $c_\gamma = 0.1$, and we take $\rho_{\tau\tau} = i\lambda_\tau$. Red (black) lines represent $\phi_{tt} = 0$ ($\pi/2$). The characteristics of each type of contribution are the same as the μ EDM case in Sec. III, except that each contribution is now larger by $\rho_{\tau\tau}/\rho_{\mu\mu}$. From Fig. 4 and for our benchmarks, d_τ can reach $\sim 10^{-23}$ e cm, but again falls short of Belle II sensitivity.

V. DISCUSSION

With our working assumption for ρ_{ij} given in Eq. (5) and sub-TeV exotic scalars, we find that μ and τ EDM can be enhanced in g2HDM, but are not large enough to be probed in the coming years. However, recent progress in muon $g-2$ may suggest good prospects for μ EDM.

The Fermilab Muon $g-2$ experiment [15] reported recently their first measurement of the muon anomalous magnetic moment, $a_\mu \equiv (g-2)_\mu$, confirming the old BNL result [53]. The combined value of $a_\mu^{\text{Exp}} = 116592061(41) \times 10^{-11}$ disagrees with the SM prediction, $a_\mu^{\text{SM}} = 116591810(43) \times 10^{-11}$ [54], by more than 4σ ,

$$a_\mu^{\text{Exp}} - a_\mu^{\text{SM}} = (251 \pm 59) \times 10^{-11}. \quad (19)$$

One of the simplest (and easiest, thanks to the chiral enhancement factor of $m_\tau/m_\mu \simeq 17$) NP explanation of Eq. (19) is provided by g2HDM via the same diagram as in Fig. 1. But it would require significant departure from Eq. (5) for some couplings. As shown in Ref. [38], to explain Eq. (19) at 1σ , one needs $|\rho_{\tau\mu}| = |\rho_{\mu\tau}| \simeq \mathcal{O}(20)\lambda_\tau$, with m_H and m_A sub-TeV but nondegenerate.

Several implications, relevant for the present paper, follow. First, one has to adopt [38] near-perfect alignment, i.e. $c_\gamma \rightarrow 0$. Though odd, it is needed to satisfy the CMS limit of $\mathcal{B}(h \rightarrow \tau\mu) < 0.15\%$ [55], which

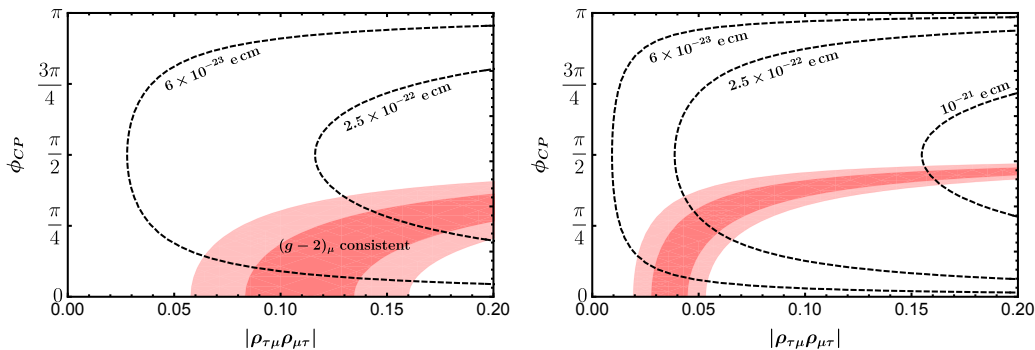


FIG. 5. Correlation between muon $g - 2$ and μ EDM. Pink (light pink) region shows parameter space that explain Eq. (19) at 1σ (2σ), while dashed lines are d_μ contours. The left (right) plot is for $c_\gamma = 0$, $m_H = 300$ GeV and $m_A = 340$ (500) GeV. All other ρ_{ij} are set to zero.

constrains $|\rho_{\tau\mu}c_\gamma| < 0.1\lambda_\tau$ for $\rho_{\tau\mu} = \rho_{\mu\tau}$. This bound implies $c_\gamma < 0.005$ for 1σ solution of muon $g - 2$. Another important implication is a rather small ρ_{tt} . The decay $\tau \rightarrow \mu\gamma$ arises from Fig. 2 with initial μ replaced by τ , which constrains the product $\rho_{\tau\mu}\rho_{tt}$. To comply with the Belle bound of $\mathcal{B}(\tau \rightarrow \mu\gamma) < 4.2 \times 10^{-8}$ [56], large $\rho_{\tau\mu}$ means small ρ_{tt} . Even more surprising [38] is that the collider search for $gg \rightarrow H, A \rightarrow \tau\mu$ provides a much better constraint. Combining both flavor and LHC constraints, ρ_{tt} seems limited to small values $\rho_{tt} \lesssim 0.1$, which is small compared with $\lambda_t \cong 1$.

Small ρ_{tt} and c_γ will suppress the two-loop contributions to ℓ EDM: the top-loop diagrams by small ρ_{tt} , and W -loop diagrams by $c_\gamma \rightarrow 0$. But large $\rho_{\tau\mu}(\rho_{\mu\tau})$ values can give rather large μ EDM via the one-loop diagram.

Defining $\rho_{\tau\mu}\rho_{\mu\tau} = |\rho_{\tau\mu}\rho_{\mu\tau}|\exp(\phi_{CP})$, we illustrate in Fig. 5 the range of d_μ accessible in the $|\rho_{\tau\mu}\rho_{\mu\tau}|$ - ϕ_{CP} plane while simultaneously accounting for muon $g - 2$, Eq. (19). The left plot is for $m_H = 300$ GeV and $m_A = 340$ GeV, which are not far from degenerate, while the right plot is for the same m_H but a much heavier $m_A = 500$ GeV. We see from both plots that, given the complexity of $\rho_{\tau\mu}\rho_{\mu\tau}$, the solution space for muon $g - 2$ projects large d_μ values that are well within PSI sensitivity! In the more optimistic scenario where m_H and m_A are farther apart, the parameter space in the right plot may even appear to be within reach of Fermilab and J-PARC muon $g-2$ experiments, namely $\sim 10^{-21}$ e cm. We caution, however, that this would demand *very* large $|\rho_{\tau\mu}| \sim |\rho_{\mu\tau}|$ values.

On the other hand, one does not expect such extraordinary enhancements for d_τ . In fact, if muon $g - 2$ arises from g2HDM as described, then d_τ will be much smaller than our estimates in Sec. IV. This is because the two-loop contribution to d_τ in Eq. (18) becomes suppressed by small ρ_{tt} and c_γ , as argued previously. Furthermore, one-loop enhancement similar to μ EDM is not possible because simultaneously large $\rho_{\tau\tau}$ and $\rho_{\tau\mu}(\rho_{\mu\tau})$ would make $\tau \rightarrow \mu\gamma$ too large at one-loop and violate the Belle bound, as we showed recently in Ref. [57].

What about e EDM? The leading one-loop results (τ in the loop) for e EDM are given by Eq. (9), replac-

ing “ μ ” \rightarrow “ e ”. Therefore, at one loop, d_e is proportional to $\text{Im}(\rho_{\tau e}\rho_{e\tau})$. The $\mu \rightarrow e\gamma$ process constrains $\rho_{\tau e}(\rho_{e\tau})$ severely. For values of $\rho_{\tau\mu}$ consistent with muon $g - 2$ solution, the current MEG [58] bound of $\mathcal{B}(\mu \rightarrow e\gamma) < 4.2 \times 10^{-13}$ gives $|\rho_{\tau e}| = |\rho_{e\tau}| \lesssim \mathcal{O}(\lambda_e)$ [57], which is in line with our working assumption in Eq. (5). Taking $|\text{Im}(\rho_{\tau e}\rho_{e\tau})| \simeq \lambda_e^2$, $c_\gamma = 0$, and $m_H = 300$ GeV and $m_A = 500$ GeV, we find $|d_e| \lesssim 5 \times 10^{-32}$ e cm, which is more than two orders of magnitude below the current ACME bound, $|d_e| < 1.1 \times 10^{-29}$ e cm. For m_H closer to m_A , d_e will be further suppressed. The two-loop results for d_e can be obtained by replacing “ μ ” \rightarrow “ e ” in the corresponding expressions for μ EDM in Sec. III. If one assumes $\rho_{ee} \sim 0$, then two-loop diagrams for e EDM is essentially given by the second term of Eq. (12) (after obvious change of lepton indices), which depends on $|s_{2\gamma} \text{Im} \rho_{tt}|$ and m_H . For $m_H = 300$ GeV, we find $|d_e| \simeq 2 \times 10^{-27} |s_{2\gamma} \text{Im} \rho_{tt}|$ e cm. With both parameters constrained to be small, $c_\gamma < 0.005$ and $|\rho_{tt}| \lesssim 0.1$, it is rather easy to satisfy the current ACME bound, without resort to the cancellation mechanism [9] to evade the experimental bound. It remains to be seen whether parameter space exists where simultaneously small ρ_{tt} and c_γ can still provide solutions to BAU in g2HDM.

VI. CONCLUSION

We study one- and two-loop mechanisms for charged lepton EDM in g2HDM, the two Higgs doublet model that possesses extra Yukawa couplings. We find both d_μ and d_τ can be enhanced to considerably larger values — thanks to the extra top Yukawa coupling $\rho_{tt} \sim \mathcal{O}(1)$.

The question for g2HDM is how it has managed to hide so well from scrutiny, if the exotics Higgs bosons are sub-TeV in mass. This we have elucidated in a previous work [32], where we developed Eq. (5) as our working assumption for the strength of extra ρ_{ij}^f couplings, namely $\rho_{ii} \lesssim \mathcal{O}(\lambda_i)$, $\rho_{1i} \lesssim \mathcal{O}(\lambda_1)$, and $\rho_{3j} \lesssim \mathcal{O}(\lambda_3)$ for $j \neq 1$. It reflects the mass-mixing hierarchies observed in the SM

sector [6], and finds further support from the cancellation mechanism [9], or interplay between ρ_{ee} and ρ_{tt} to satisfy the recent ACME 2018 bound on d_e , while ρ_{tt} still drives baryogenesis. Flavor changing couplings of $h(125)$ are further suppressed by the recent emergent phenomenon of alignment, i.e. small h - H mixing.

With our working assumption as above and taking central values, we showed that d_μ lies in the ballpark range of 10^{-24} e cm, while d_τ is in the 10^{-23} e cm range. These numbers could go up by another order of magnitude as allowed by Eq. (5). But though they are much larger than typical expectations in MFV-like scenarios, with future sensitivities as stated in Table 1, it is unlikely that d_μ and d_τ would be observed in the near future. Thus, Eq. (5) continues to “protect” g2HDM from revealing itself, and we have advocated elsewhere for LHC direct search [30], as well as several flavor probes [32].

The recent experimental affirmation of the muon $g-2$ “anomaly”, however, brings in some hope, but at a cost.

In g2HDM, the one-loop mechanism can quite simply account for the discrepancy, if $|\rho_{\tau\mu}| \simeq |\rho_{\mu\tau}| = \mathcal{O}(20\lambda_\tau) \sim 0.2$. This would grossly violate our working assumption of Eq. (5); but *Nature* herself is the judge and the jury, and maybe this is what she has been telling us through the “anomaly”. The point is, the same one-loop diagram can generate d_μ through the complexity of $\rho_{\tau\mu}\rho_{\mu\tau}$, which *can* be tested with projected experimental sensitivities. But this single-enhanced coupling scenario would then imply quite small $\rho_{tt} \lesssim 0.1$, while alignment must be near-perfect, which by themselves are rather peculiar. These in turn suggest that d_τ will be rather suppressed, and d_e can be much below ACME bound without resort to cancellation mechanism.

Acknowledgments This research is supported by MOST 109-2112-M-002-015-MY3, 110-2639-M-002-002-ASP and 110-2811-M-002-620 of Taiwan, and NTU grants 110L104019 and 110L892101.

-
- [1] N. Cabibbo, Phys. Rev. Lett. **10**, 531 (1963).
 [2] M. Kobayashi and T. Maskawa, Prog. Theor. Phys. **49**, 652 (1973).
 [3] A.D. Sakharov, Pisma Zh. Eksp. Teor. Fiz. **5**, 32 (1967).
 [4] G.C. Branco, P.M. Ferreira, L. Lavoura, M.N. Rebelo, M. Sher and J.P. Silva, Phys. Rept. **516**, 1 (2012) [arXiv:1106.0034 [hep-ph]].
 [5] S. Davidson and H.E. Haber, Phys. Rev. D **72**, 035004 (2005) [erratum: Phys. Rev. D **72**, 099902 (2005)] [arXiv:hep-ph/0504050].
 [6] W.-S. Hou, Phys. Lett. B **296**, 179 (1992).
 [7] S.L. Glashow and S. Weinberg, Phys. Rev. D **15**, 1958 (1977).
 [8] K. Fuyuto, W.-S. Hou and E. Senaha, Phys. Lett. B **776**, 402 (2018) [arXiv:1705.05034 [hep-ph]].
 [9] K. Fuyuto, W.-S. Hou and E. Senaha, Phys. Rev. D **101**, 011901 (2020) [arXiv:1910.12404 [hep-ph]].
 [10] M. Pospelov and A. Ritz, Annals Phys. **318**, 119-169 (2005) [arXiv:hep-ph/0504231].
 [11] M. Pospelov and A. Ritz, Phys. Rev. D **89**, 056006 (2014) [arXiv:1311.5537 [hep-ph]].
 [12] C. Smith and S. Touati, Nucl. Phys. B **924**, 417-452 (2017) [arXiv:1707.06805 [hep-ph]].
 [13] J. Baron *et al.* [ACME], Science **343**, 269 (2014) [arXiv:1310.7534 [physics.atom-ph]].
 [14] V. Andreev *et al.* [ACME], Nature **562**, 355 (2018).
 [15] B. Abi *et al.* [Muon $g-2$], Phys. Rev. Lett. **126**, 141801 (2021) [arXiv:2104.03281 [hep-ex]].
 [16] G.W. Bennett *et al.* [Muon ($g-2$)], Phys. Rev. D **80**, 052008 (2009) [arXiv:0811.1207 [hep-ex]].
 [17] Y. Ema, T. Gao and M. Pospelov, arXiv:2108.05398 [hep-ph].
 [18] R. Chislett [Muon $g-2$], EPJ Web Conf. **118**, 01005 (2016).
 [19] M. Abe *et al.*, PTEP **2019**, 053C02 (2019) [arXiv:1901.03047 [physics.ins-det]].
 [20] A. Adelmann *et al.*, [arXiv:2102.08838 [hep-ex]].
 [21] K. Inami *et al.* [Belle], Phys. Lett. B **551**, 16 (2003) [arXiv:hep-ex/0210066].
 [22] K. Inami, K. Hayasaka *et al.* [Belle], arXiv:2108.11543 [hep-ex].
 [23] E. Kou *et al.* [Belle-II], PTEP **2019**, 123C01 (2019) [erratum: PTEP **2020**, 029201 (2020)] [arXiv:1808.10567 [hep-ex]].
 [24] W. Bernreuther, L. Chen and O. Nachtmann, Phys. Rev. D **103**, 096011 (2021) [arXiv:2101.08071 [hep-ph]].
 [25] G. D’Ambrosio, G.F. Giudice, G. Isidori and A. Strumia, Nucl. Phys. B **645**, 155 (2002) [arXiv:hep-ph/0207036].
 [26] G. Hiller, K. Huitu, T. Ruppel and J. Laamanen, Phys. Rev. D **82**, 093015 (2010) [arXiv:1008.5091].
 [27] A. Crivellin, M. Hoferichter and P. Schmidt-Wellenburg, Phys. Rev. D **98**, 113002 (2018) [arXiv:1807.11484 [hep-ph]].
 [28] W.-S. Hou and M. Kikuchi, EPL **123**, 11001 (2018) [arXiv:1706.07694 [hep-ph]].
 [29] A. Crivellin, A. Kokulu and C. Greub, Phys. Rev. D **87**, 094031 (2013) [arXiv:1303.5877 [hep-ph]].
 [30] W.-S. Hou and T. Modak, Mod. Phys. Lett. A **36**, 2130006 (2021) [arXiv:2012.05735 [hep-ph]].
 [31] W.-S. Hou and G. Kumar, Phys. Rev. D **101**, 095017 (2020) [arXiv:2003.03827 [hep-ph]].
 [32] W.-S. Hou and G. Kumar, Phys. Rev. D **102**, 115017 (2020) [arXiv:2008.08469 [hep-ph]].
 [33] G. Aad *et al.* [ATLAS], Phys. Lett. B **812**, 135980 (2021) [arXiv:2007.07830 [hep-ex]].
 [34] A.M. Sirunyan *et al.* [CMS], JHEP **01**, 148 (2021) [arXiv:2009.04363 [hep-ex]].
 [35] J.R. Dell’Aquila and C.A. Nelson, Nucl. Phys. B **320**, 61 (1989).
 [36] R. Harnik, A. Martin, T. Okui, R. Primulando and F. Yu, Phys. Rev. D **88**, 076009 (2013) [arXiv:1308.1094 [hep-ph]].
 [37] The CMS Collaboration, CMS-PAS-HIG-20-006.
 [38] W.-S. Hou, R. Jain, C. Kao, G. Kumar and T. Modak, [arXiv:2105.11315 [hep-ph]].
 [39] Y. Omura, E. Senaha and K. Tobe, Phys. Rev. D **94**, 055019 (2016) [arXiv:1511.08880 [hep-ph]].
 [40] S.M. Barr and A. Zee, Phys. Rev. Lett. **65**, 21 (1990)

- [erratum: Phys. Rev. Lett. **65**, 2920 (1990)].
- [41] J. D. Bjorken and S. Weinberg, Phys. Rev. Lett. **38**, 622 (1977)
- [42] R.G. Leigh, S. Paban and R.-M. Xu, Nucl. Phys. B **352**, 45 (1991).
- [43] D. Chang, W.-Y. Keung and T.-C. Yuan, Phys. Rev. D **43**, R14 (1991).
- [44] C. Kao and R.-M. Xu, Phys. Lett. B **296**, 435 (1992).
- [45] D. Bowser-Chao, D. Chang and W.-Y. Keung, Phys. Rev. Lett. **79**, 1988 (1997) [arXiv:hep-ph/9703435].
- [46] T. Abe, J. Hisano, T. Kitahara and K. Tobioka, JHEP **01**, 106 (2014) [erratum: JHEP **04**, 161 (2016)] [arXiv:1311.4704 [hep-ph]].
- [47] J.F. Gunion and H.E. Haber, Phys. Rev. D **67**, 075019 (2003) [arXiv:hep-ph/0207010].
- [48] S. Davidson and G.J. Grier, Phys. Rev. D **81**, 095016 (2010) [arXiv:1001.0434 [hep-ph]].
- [49] S. Inoue, M.J. Ramsey-Musolf and Y. Zhang, Phys. Rev. D **89**, no.11, 115023 (2014) [arXiv:1403.4257].
- [50] E.J. Chun, J. Kim and T. Mondal, JHEP **12**, 068 (2019) [arXiv:1906.00612].
- [51] W. Altmannshofer, S. Gori, N. Hamer and H.H. Patel, Phys. Rev. D **102**, 115042 (2020) [arXiv:2009.01258].
- [52] D. Egana-Ugrinovic and S. Thomas, [arXiv:1810.08631 [hep-ph]].
- [53] G.W. Bennett *et al.* [Muon g-2], Phys. Rev. D **73**, 072003 (2006) [arXiv:hep-ex/0602035].
- [54] T. Aoyama *et al.*, Phys. Rept. **887**, 1 (2020) [arXiv:2006.04822 [hep-ph]].
- [55] A.M. Sirunyan *et al.* [CMS], [arXiv:2105.03007 [hep-ex]].
- [56] A. Abdesselam *et al.* [Belle], [arXiv:2103.12994 [hep-ex]].
- [57] W.-S. Hou and G. Kumar, [arXiv:2107.14114 [hep-ph]].
- [58] A.M. Baldini *et al.* [MEG], Eur. Phys. J. C **76**, 434 (2016) [arXiv:1605.05081 [hep-ex]].
- [59] M. Jung and A. Pich, JHEP **04**, 076 (2014) [arXiv:1308.6283 [hep-ph]].

Appendix A

Below we provide Barr-Zee formulae related to $d_\mu^{\phi Z}$ and charged Higgs loop, together with expressions for all the loop functions used for calculation of EDMs in this paper.

1. More Barr-Zee formulae

The Barr-Zee formulae for $d_\mu^{\phi Z}$ are as follows. Similar to $d_\mu^{\phi\gamma}$, we decompose the top-loop contributions to $d_\mu^{\phi Z}$ as $(d_\mu^{\phi Z})_t = (d_\mu^{\phi Z})_t^{\text{mix}} + (d_\mu^{\phi Z})_t^{\text{extra}}$. The expressions for each term are,

$$(d_\mu^{\phi Z})_t^{\text{mix}} = \frac{e \alpha s_{2\gamma}}{256\pi^3 m_t s_W^2 c_W^2} (1 - 4s_W^2)(1 - \frac{8}{3}s_W^2) \left\{ \left[\lambda_t \text{Im } \rho_{\mu\mu} \left(\frac{m_h^2 f(x_{th}) - m_Z^2 f(x_{tZ})}{m_h^2 - m_Z^2} - h \rightarrow H \right) \right] + \left[\lambda_\mu \text{Im } \rho_{tt} \left(f \rightarrow g \right) \right] \right\}, \quad (\text{A1})$$

$$(d_\mu^{\phi Z})_t^{\text{extra}} = \frac{e \alpha}{128\pi^3 m_t s_W^2 c_W^2} (1 - 4s_W^2)(1 - \frac{8}{3}s_W^2) \left\{ \left[\text{Im } \rho_{\mu\mu} \text{Re } \rho_{tt} \left(c_\gamma^2 \frac{m_h^2 f(x_{th}) - m_Z^2 f(x_{tZ})}{m_h^2 - m_Z^2} + s_\gamma^2 \frac{m_H^2 f(x_{tH}) - m_Z^2 f(x_{tZ})}{m_H^2 - m_Z^2} + \frac{m_A^2 g(x_{tA}) - m_Z^2 g(x_{tZ})}{m_A^2 - m_Z^2} \right) \right] + \left[\text{Im } \rho_{tt} \text{Re } \rho_{\mu\mu} \left(f \leftrightarrow g \right) \right] \right\}, \quad (\text{A2})$$

The W -loop contribution is,

$$(d_\mu^{\phi Z})_W = -\frac{e \alpha s_\gamma c_\gamma (1 - 4s_W^2)}{128\sqrt{2}\pi^3 v s_W^2} \text{Im } \rho_{\mu\mu} \left[I_Z(m_h) - I_Z(m_H) \right], \quad (\text{A3})$$

and lastly, the charged Higgs loop diagram gives,

$$(d_\mu^{\phi Z})_{H^+} = -\frac{e \alpha (c_W^2 - s_W^2)(1 - 4s_W^2)}{256\sqrt{2}\pi^3 v s_W^2 c_W^2} \text{Im } \rho_{\mu\mu} \left[c_\gamma C_{hH^+H^-} I_3^Z(m_H^+, m_h) - s_\gamma C_{HH^+H^-} I_3^Z(m_H^+, m_H) \right], \quad (\text{A4})$$

where the trilinear couplings $\phi H^+ H^-$ are defined as $-ivC_{\phi H^+ H^-}$ in notation of Refs. [47, 48]. Note that $C_{AH^+ H^-} = 0$.

The charged Higgs loop contribution for $d_\mu^{\phi\gamma}$ and $d_\mu^{H^\pm W^\pm}$ are,

$$(d_\mu^{\phi\gamma})_{H^+} = -\frac{e\alpha}{32\sqrt{2}\pi^3 v} \text{Im} \rho_{\mu\mu} \left[c_\gamma C_{hH^+H^-} I_3^\gamma(m_H^+, m_h) - s_\gamma C_{HH^+H^-} I_3^\gamma(m_H^+, m_H) \right], \quad (\text{A5})$$

$$(d_\mu^{H^+W^+})_{H^+} = -\frac{e}{256\sqrt{2}\pi^4 v} \text{Im} \rho_{\mu\mu} \left[c_\gamma C_{hH^+H^-} \mathcal{I}_5(m_h, m_H^+) - s_\gamma C_{HH^+H^-} \mathcal{I}_5(m_H, m_H^+) \right]. \quad (\text{A6})$$

2. Loop Functions

The loop functions appearing in various Barr-Zee formulae of lepton EDM are listed below. The functions appearing in top quark contribution to $d_\mu^{\phi\gamma}$ and $d_\mu^{\phi Z}$ are [40],

$$f(a) = a \int_0^1 dz \frac{1/2 - z + z^2}{z(1-z) - a} \log \frac{z(1-z)}{a}, \quad g(a) = \frac{a}{2} \int_0^1 dz \frac{1}{z(1-z) - a} \log \frac{z(1-z)}{a}. \quad (\text{A7})$$

The functions appearing in W -loop contribution to $d_\mu^{\phi\gamma}$ and $d_\mu^{\phi Z}$ are [46],

$$I_V(m_\phi) = \frac{m_W^2}{m_\phi^2 - m_V^2} \left\{ \left[6 - \frac{m_V^2}{m_W^2} + \left(1 - \frac{m_V^2}{2m_W^2} \right) \frac{m_\phi^2}{m_W^2} \right] \left(\frac{m_\phi^2}{m_W^2} f(m_W^2/m_\phi^2) - \frac{m_V^2}{m_W^2} f(m_W^2/m_V^2) \right) \right. \\ \left. - \left[-10 + \frac{3m_V^2}{m_W^2} + \left(1 - \frac{m_V^2}{2m_W^2} \right) \frac{m_\phi^2}{m_W^2} \right] \left(\frac{m_\phi^2}{m_W^2} g(m_W^2/m_\phi^2) - \frac{m_V^2}{m_W^2} g(m_W^2/m_V^2) \right) \right\}. \quad (\text{A8})$$

The functions appearing in H^+ -loop contribution to $d_\mu^{\phi\gamma}$ and $d_\mu^{\phi Z}$ are [46],

$$I_3^V(m_H^+, m_\phi) = \frac{v^2}{m_\phi^2 - m_V^2} \left\{ \left[\frac{m_V^2}{m_{H^+}^2} \left(f(m_{H^+}^2/m_V^2) - g(m_{H^+}^2/m_V^2) \right) \right] - \left[V \rightarrow \phi \right] \right\}. \quad (\text{A9})$$

The functions appearing in fermion loop contributions to $d_\mu^{H^+W^+}$ are [45, 59],

$$F_q(a, b) = \frac{T_q(a) - T_q(b)}{a - b}; \quad q = t, b, \quad (\text{A10})$$

where

$$T_b(a) = \frac{1 - 3a}{a^2} \frac{\pi^2}{6} + \left(\frac{1}{a} - \frac{5}{2} \right) \log a - \frac{1}{a} - \left(2 - \frac{1}{a} \right) \left(1 - \frac{1}{a} \right) \text{Li}_2(1-a), \quad (\text{A11})$$

$$T_b(a) = \frac{2a - 1}{a^2} \frac{\pi^2}{6} + \left(\frac{3}{2} - \frac{1}{a} \right) \log a + \frac{1}{a} - \frac{1}{a} \left(2 - \frac{1}{a} \right) \text{Li}_2(1-a). \quad (\text{A12})$$

Finally, the functions appearing in diagrams with W^+ and H^+ loops for $d_\mu^{H^+W^+}$ are [46],

$$\mathcal{I}_{4(5)}(m_\phi, m_{H^+}) = \frac{m_W^2}{m_{H^+}^2 - m_W^2} \left[\mathcal{I}_{4(5)}(m_W, m_\phi) - \mathcal{I}_{4(5)}(m_{H^+}, m_\phi) \right], \quad (\text{A13})$$

where,

$$I_4(m_i, m_\phi) = \int_0^1 dz \frac{m_i^2 \left(z(1-z)^2 - 4(1-z)^2 + \frac{m_{H^+}^2 - m_\phi^2}{m_W^2} z(1-z)^2 \right)}{m_W^2(1-z) + m_\phi^2 z - m_i^2 z(1-z)} \log \left(\frac{m_W^2(1-z) + m_\phi^2 z}{m_i^2 z(1-z)} \right), \quad (\text{A14})$$

$$I_5(m_i, m_\phi) = 2 \int_0^1 dz \frac{m_i^2 z(1-z)^2}{m_{H^+}^2(1-z) + m_\phi^2 z - m_i^2 z(1-z)} \log \left(\frac{m_{H^+}^2(1-z) + m_\phi^2 z}{m_i^2 z(1-z)} \right). \quad (\text{A15})$$